Journal of Solid State Chemistry **143,** 86–94 (1999)
Article ID jssc.1998.8087, available online at http://www.idealibrary.com on IDEAL®

In Situ Coupled Raman and Impedance Measurements of the Reactivity of Nanocrystalline SnO_2 versus H_2S

T. Pagnier,*,[1] M. Boulova,† A. Galerie,‡ A. Gaskov,† and G. Lucazeau*

*Laboratoire d'Electrochimie et de Physicochimie des Matériaux et Interfaces, UMR INPG-CNRS, ENSEEG BP 75, 38402 Saint Martin d'Hères, France; †Laboratory of Diagnostic of Inorganic Materials, Chemistry Department, Moscow State University, Leninskie Gory, 119899 Moscow, Russia; and ‡Laboratoire de Thermodynamique et dePhysico Chimie des Matériaux, UMR INPG-CNRS, ENSEEG BP 75, 38402 Saint Martin d'Hères, France

Received April 13, 1998; in revised form November 4, 1998; accepted November 8, 1998

Nanocrystalline SnO_2 produced in different ways has been subjected to H_2S at 100°C. The formation of SnS_x was deduced from Raman spectra and correlated with the changes in electrical resistance. When the initial resistance of the sample was high, adsorbed SO_4 was observed. The agreement of these results with available thermodynamic data and the actual theory of SnO_2 sensitivity to H_2S is discussed. © 1999 Academic Press

INTRODUCTION

Tin oxide SnO_2 is extensively studied as a base material for its gas sensor applications. It is oxygen deficient and therefore is an *n*-type semiconductor with a wide bandgap (3.6 eV) (1). In contact with air, polycrystalline SnO_2 adsorbs O_2 molecules (2) which act as electron acceptors and therefore create a depletion layer around each grain (3–5). Traces of foreign gases (H_2, CO, H_2S, NO, ...) affect the adsorbed oxygen coverage which leads to a decrease in the sample resistance (3, 6–11). The effect of crystallite size on the sensing properties has been widely studied (8–11). Nanocrystalline powders have attracted considerable interest because of their high sensitivity. In a recent paper, we have presented the Raman spectra of various nanocrystalline SnO_2 powders (12). In this paper, we present the results of our investigations on the reaction of nanocrystalline SnO_2 with H_2S by combined Raman spectroscopy and electrical measurements.

1. EXPERIMENTAL

1.1. Sample Preparation

Four SnO_2 materials were used: a commercial microcrystalline SnO_2 powder (Prolabo), a nanocrystalline powder (sample SV6), and two pellets prepared with nanocrystalline SnO_2 powders (samples SK and SX). SV6 and SK were prepared according to route II of (12) while SX was prepared by route I. Route I consists in the precipitation of stannic acid and in the treatment of sodium stannate in H^+ resin; the obtained colloidal solution is then freeze-dried in a sublimator and calcined at 600°C. Route II starts with the classical hydrolysis of $SnCl_4$ to obtain the precipitation of stannic acid folllowed by washing, drying at 100°C, and calcination. Pellets (diameter 6 mm, thickness 2 mm) SK and SX were then pressed at 700 MPa and sintered at 700°C for 4 h in air. The final density of the pellets was 40% of the theoretical one. SEM observations (12) indicate the presence of 3D aggregates for powders obtained with route I and the presence of 2D aggregates for powders obtained with route II.

1.2. Experimental Setup

Combined electrical measurements and Raman spectroscopy were made in a specific cell allowing atmosphere control. The cell is schematically shown in Fig. 1. The cell body is made with 316 L stainless steel. The cover of the cell was equipped with a quartz window for Raman experiments. Samples were placed in an alumina crucible. Flowing gas was either dry air (80% N_2, 20% O_2) or 300 ppm H_2S in N_2. For electrical measurements, two silver electrodes were painted on the top face of the pellets. Two thin silver wires were attached to the electrodes with the same paint.

Raman spectra were collected in the backscattering geometry through a 50× objective. The excitation light was the 514.5 nm green light of an Ar laser. A Dilor XY Raman spectrometer equipped with a cooled CCD detector was used. Raman spectra were generally collected at the same point of a sample during atmospheric cycles. However, some measurements were sometimes rapidly performed at various points when changes in the Raman spectra were slow. Raman spectra were independent of the

[1] To whom correspondence should be sent.

0022-4596/99 $30.00

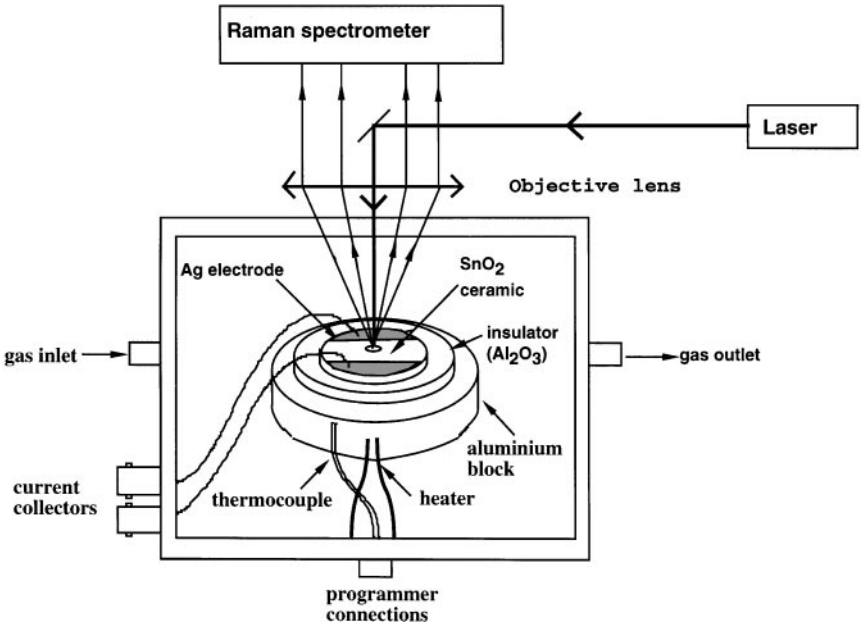

FIG. 1. Schematic diagram of the experimental setup.

measuring position, and particularly of the distance to the electrodes.

Electrical measurements were first performed with a Solartron 1260 impedance meter. As it became rapidly clear that in all cases impedance spectra solely consisted of a setup capacitance in parallel with a true sample resistance, a digital ohmmeter (Fluke 87) was used instead.

Most experiments were carried out at 100°C.

2. RESULTS

2.1. Initial Spectra

Figure 2 shows the initial Raman spectra of all samples at 100°C in air. The spectrum of microcrystalline SnO_2 corresponds to the rutile structure. Three out of four Raman active modes can be seen with symmetry E_g (476 cm^{-1}), A_{1g} (618 cm^{-1}) and B_{2g} (772 cm^{-1}). The B_{1g} mode wavenumber is too low for it to appear in the figure. Nanocrystalline powders exhibit the A_{1g} line and extra lines around it which have been attributed to surface modes (12). Sample SK also exhibits a strong feature at 992 cm^{-1}.

2.2. Atmospheric Effects on Raman Spectra

Figure 3 shows the effect of atmosphere changes in the Raman spectra of SV6 powder at 100°C. The major effect of a first exposition to H_2S is the growth of a band at 992 cm^{-1}. Another broad and weaker band appears at about 350 cm^{-1}. After 130 min in H_2S, the atmosphere was switched to dry air. The band at 350 cm^{-1} disappears, while that at 992 cm^{-1} still grows and seems to saturate after 60 min in air. Another effect is the loss of intensity of the surface mode bands. A second exposure to H_2S has immediate and strong effects: the band at 992 cm^{-1} decreases rapidly, while that at 350 cm^{-1} increases. Bands characteristic of the surface modes recover their intensity, while the whole spectrum seems to be weaker.

Figure 4 shows the Raman spectra obtained with the pellet SK for two atmosphere cycles at 100°C. The first spectrum in air is similar to that of sample SV6, except that the band at 992 cm^{-1} is already present. H_2S exposure leads to an important loss of the whole spectrum intensity and to the appearance of a broad band at 350 cm^{-1}, which becomes the most intense feature of the spectrum. Switching back to air, the overall intensity increases again, the band at 350 cm^{-1} disappears, and the band at 992 cm^{-1} becomes much more intense. The relative intensity of the surface modes tends to decrease. A second H_2S–air cycle gives rise to the same behavior, except for the surface modes which intensity remain low. Notice that the E_g band, which was almost completely hidden by surface modes, appears clearly during this second cycle.

All these features are more clearly seen in Fig. 5, where the amplitudes have been normalized to that of the A_{1g} band. Notice in particular that the broad band centered at about 350 cm^{-1} becomes quite intense under H_2S flow (first and third spectra of Fig. 5).

Figure 6 shows some of the Raman spectra obtained on pellet SX at 100°C during one air–H_2S–air cycle. A quick look at these spectra seems to indicate that there is almost

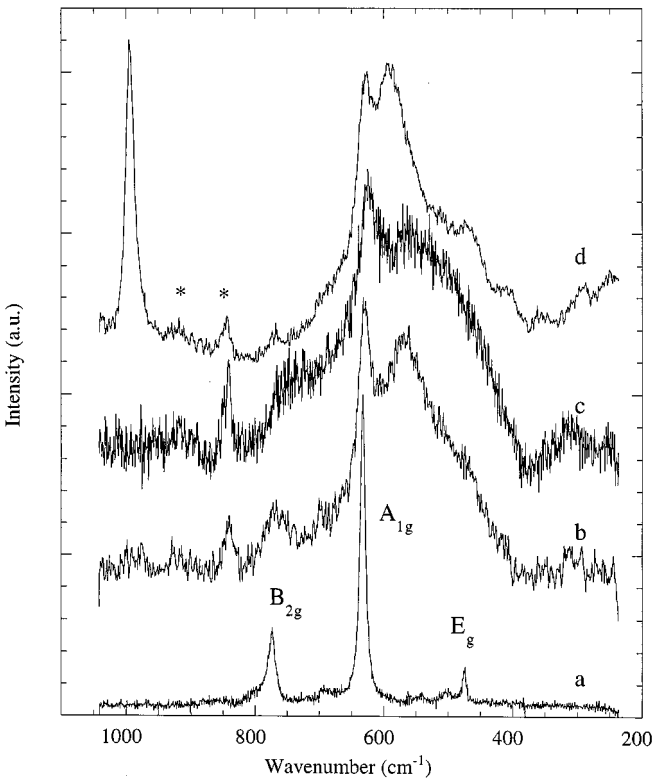

FIG. 2. Initial Raman spectra of the four samples: (a) microcrystalline SnO_2; (b) powder SV6; (c) pellet SX; (d) pellet SK. Asterisks denote fluorescence bands of the objective.

no change, except for a small decrease in overall intensity when the sample was exposed to H_2S. In the same time, the background level decreased markedly, which leads to a better signal/noise ratio. In order to put in evidence small changes, we used the following procedure: all spectra were normalized according to the A_{1g} peak. The initial spectrum (in air) was then subtracted from all other spectra. The result is shown in Fig. 7. A broad band appears at about 370 cm^{-1} in H_2S, together with a broad component at about 670 cm^{-1}. In air, the bands at 370 and 670 cm^{-1} disappear while a decrease of the surface mode intensity is observed (valley at about 580 cm^{-1}). Notice that there is no evidence for a band at 992 cm^{-1}.

Finally, Raman spectra of microcrystalline SnO_2 powder showed no change at all during multiple air–H_2S cycling.

2.3. Atmospheric Effects on Electrical Resistance

The electrical resistance and the Raman spectra of the two pellets SK and SX were monitored simultaneously. The initial resistance of the SK sample was very high ($>10^8\,\Omega$). Resistance changes at 100°C are shown in Fig. 8 (top). Clearly, the effect of H_2S exposure is a drastic decrease in the sample resistance. Immediately after air exposure, the resistance increased to a very high value.

On the contrary, the resistance of sample SX was initially low (370 Ω). When the sample was exposed to H_2S, the resistance decreased to a value of 170 Ω. It increased again when the sample was exposed to air, but quite slowly (Fig. 8 (bottom).

Also shown in Fig. 8 are the changes in the A_{1g} band amplitude. When switching from air to H_2S atmosphere, we always observe a simultaneous decrease of the resistance and of this amplitude. When switching back to air, the change in the amplitude appears systematically later than the change in resistance.

3. DISCUSSION

3.1. Assignment of the 992 and 350 cm^{-1} Bands

The band at 992 cm^{-1} strongly suggests the presence of SO_4^{2-} ions. The symmetric stretching (A_1) mode of tetrahedral SO_4^{2-} is very intense and has been found between 960 and 1020 cm^{-1} depending on the nature of the cation (17). Figure 9 shows the Raman spectrum of $SnSO_4$ that we obtained on a commercially available powder sample (Aldrich). The A_1 mode appears at 970 cm^{-1} and is much thinner in $SnSO_4$. One may think that the 992 cm^{-1} band is not due to the formation of crystalline $SnSO_4$, but to the appearance of adsorbed SO_4^{2-} ions. The strong correlation that exists between the increase of the intensity of this band and the decrease of the surface mode intensity reinforces this hypothesis.

The attribution of the 350 cm^{-1} band is not so easy. As it appears when SnO_2 is in contact with H_2S, one may think of tin sulfide. The Raman spectrum of commercial (Aldrich) SnS powder is also shown in Fig. 9. The most intense band appears at 300 cm^{-1}. As for sulfate ions, the shift could be attributed to superficial SnS. Its broadness in our SnO_2 samples could be due to some size effect, as for unreacted nanocrystalline SnO_2.

3.2. Thermodynamic Stability of Oxygen and Sulfur Containing Phases

As it has been shown that SnO_2 reacts with H_2S, it is interesting to know which phases are thermodynamically suspected to appear.

The stability diagram of tin oxide, sulfide, and sulfate phases is drawn at 400 K in Fig. 10. Thermodynamic data are from Barin (18). In such a diagram, the divariant equilibria between two solids and the gas phase are represented by straight lines with equations of the type

$$A\log(P_{S_2}) = B\log(P_{O_2}) + C, \qquad [1]$$

where $|A|$ and $|B|$ are the stoichiometric coefficients of S_2 and O_2 in the investigated reaction and $|C|$ is the $|\Delta G^0|$ of the reaction ($|\ |$ denote absolute values).

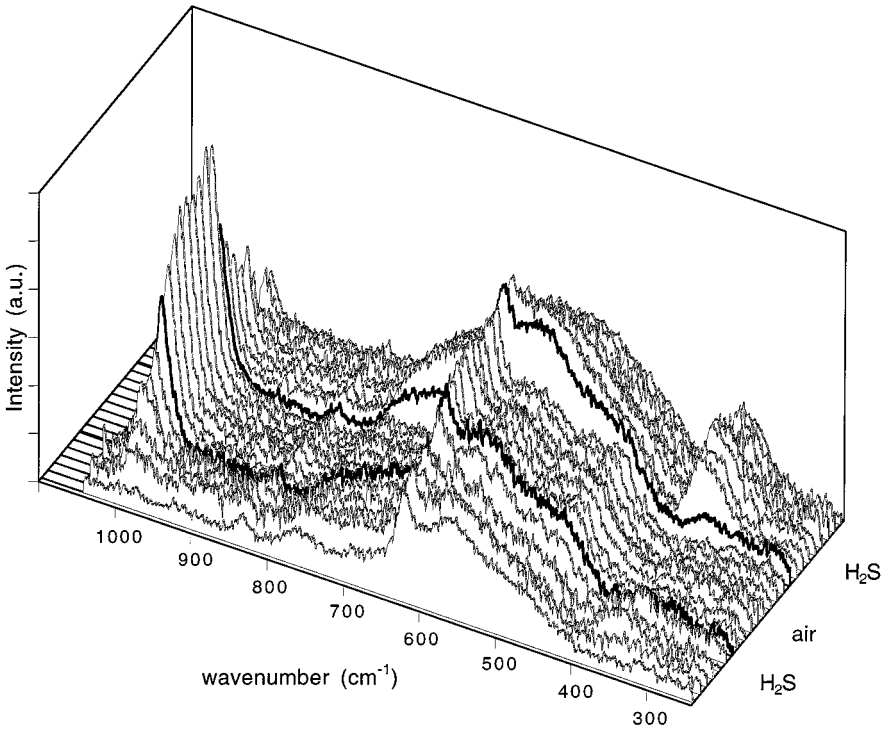

FIG. 3. Raman spectra of powder SV6 submitted to an H_2S (300 ppm in Ar)–air–H_2S cycles at 100°C. Thicker spectra are the first after atmospheric change.

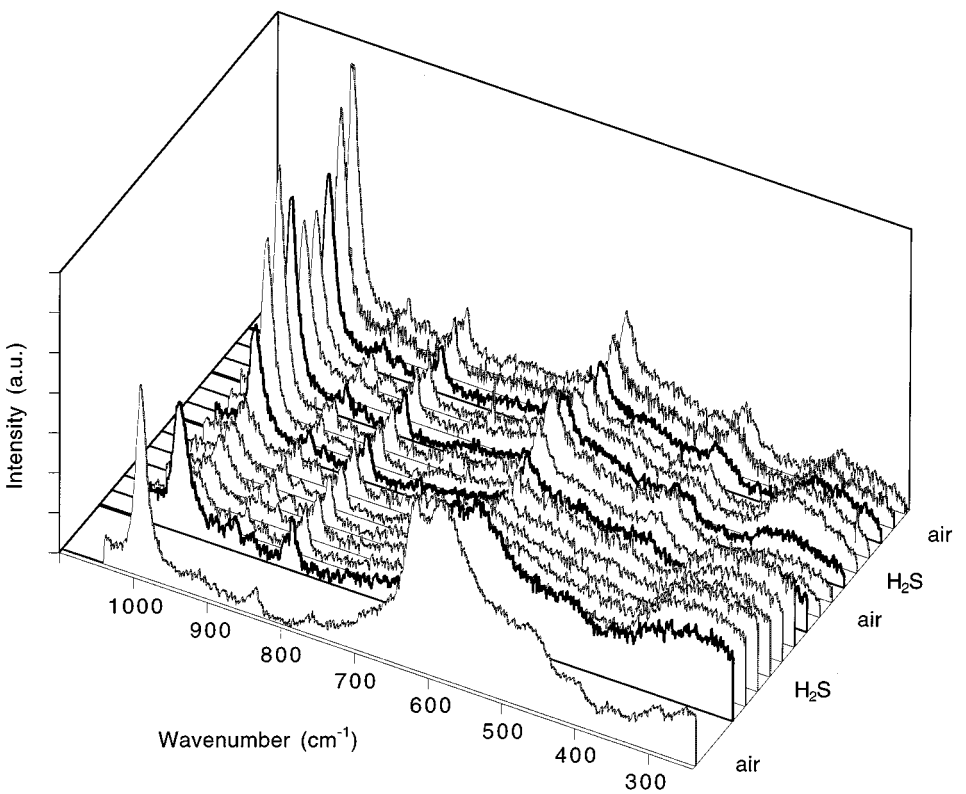

FIG. 4. Raman spectra of pellet SK submitted to two H_2S (300 ppm in Ar)–air cycles at 100°C. Thicker spectra are the first after atmospheric change.

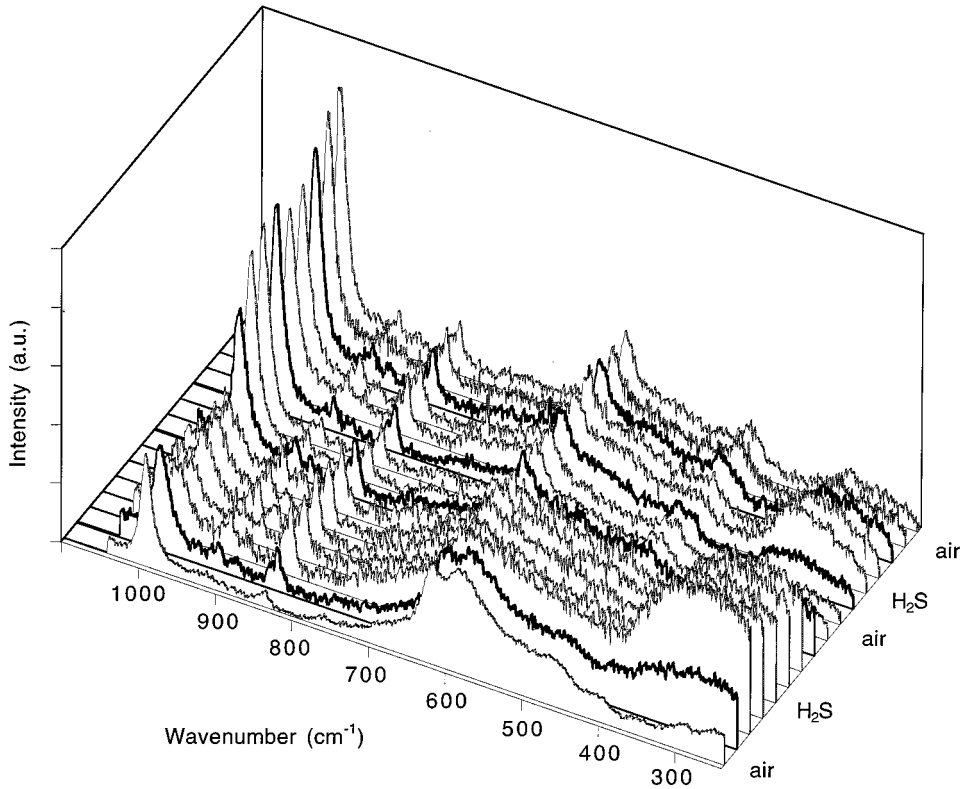

FIG. 5. Same as Fig. 4, but all spectra have been normalized so that the A_{1g} band is of the same magnitude in each spectrum.

Particular equilibria involving solely oxygen or sulfur appear as lines parallel to the axes. Univariant points of the diagram involve three solid equilibria.

In principle, the diagram is limited by the condensation of liquid sulfur for P_{S_2} higher than $10^{-8.3}$ bar. This limitation has no effect on our conclusions and was not taken into account when drawing Fig. 10.

The connexion between H_2S partial pressure and S_2 partial pressure was made with the use of the decomposition reaction of H_2S:

$$2H_2S \Leftrightarrow 2H_2 + S_2 \quad [2]$$

The continuous lines of the diagram separate six domains where one solid phase of fixed composition is stable. It is observed that SnO_2 presents a large domain of stability, even for high-S_2 pressures, provided that O_2 partial pressure is in the range of 10^{-40} bar. In the presence of sulfur SnO_2 can be transformed into sulfide by reducing P_{O_2} or saturating with Sn. On the other side, saturating SnO_2 with oxygen will result in the formation of Sn (IV) sulfate in presence of sulfur.

The metastable $SnO_2/SnSO_4$ equilibrium is represented by a dashed line in Fig. 10. It may be observed that this line is not too far from that of the $SnO_2/Sn(SO_4)_2$ equilibrium. With convenient thermodynamic conditions, $SnSO_4$ may appear in the case of a kinetically limited stannic sulfate formation.

The thermodynamic conditions imposed by the reacting gas used (300 ppm H_2S in Ar) correspond to a P_{S_2} of $10^{-3.5}$ bar (in fact, this pressure is lower as H_2S decomposition is probably very slow). The oxygen partial pressure is fixed by residual O_2 in Ar at about 10^{-5} bar. If oxygen does not react with H_2S, the working conditions correspond to point A. If oxygen reacts with H_2S according to

$$H_2S + 2O_2 \Leftrightarrow SO_3 + H_2O, \quad [3]$$

calculations at 400 K lead to $\log P_{O_2} = -7.4$ and $\log P_{SO_3} = \log P_{H_2O} = -5.3$ (point B). In all cases, the sulfate phase is the stable one.

It is therefore not surprising that the Raman spectrum of SO_4^{2-} appears in H_2S atmosphere. The presence of tin sulfide (SnS or SnS_2) is more questionable from a thermodynamic point of view. Their appearance suggests that locally the partial pressure of oxygen is much lower than in the gas phase. The formation of sulfide could also be assisted by the fact that nanocrystallites have a smaller enthalpy of formation than larger crystals.

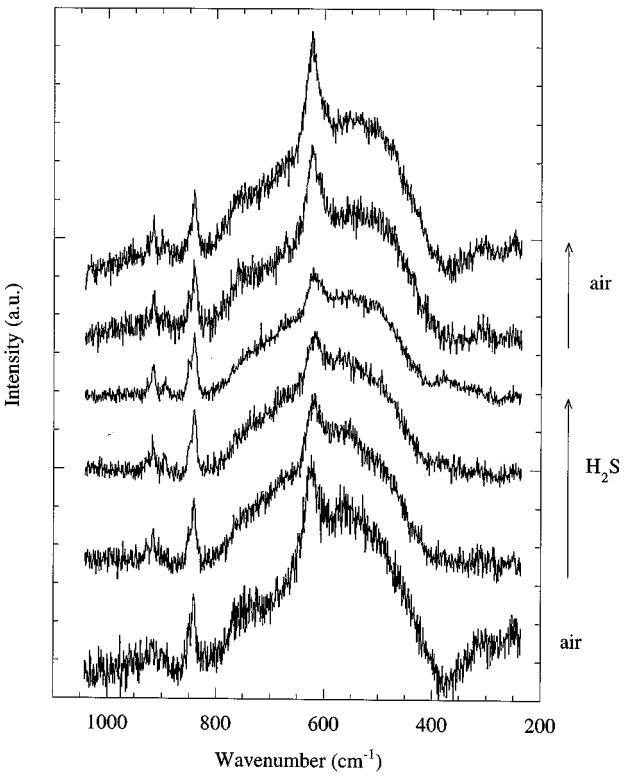

FIG. 6. Raman spectra of pellet SX submitted to an H_2S (300 ppm in Ar)–air–H_2S cycle at 100°C.

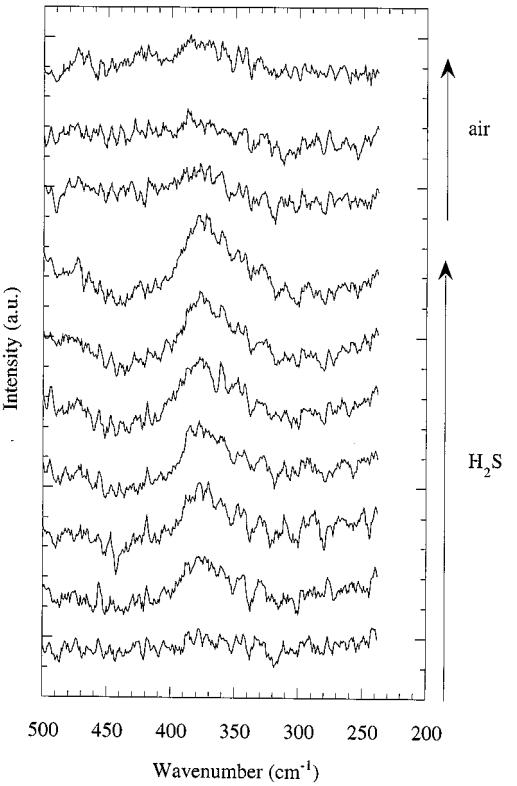

FIG. 7. Difference Raman spectra of pellet SX submitted to an H_2S (300 ppm in Ar)–air–H_2S cycle at 100°C. Spectra were first normalized so that the A_{1g} band is of the same amplitude. The first spectrum in air was then subtracted from all other spectra.

3.3. Initial Conductivity of the Samples

The electrical conductivity of SnO_2 has been the subject of numerous investigations. It is highly sensitive to non-stoichiometry, impurities, microstructure and surrounding atmosphere. From single crystal experiments (1, 13), one can deduce that the maximum electrical conductivity of SnO_2 is $0.3\,\Omega^{-1}\,cm^{-1}$ at 300 K. In polycrystalline materials or thin films, the conductivity, when given, is much lower (8). This phenomenon is attributed to the adsorption of O_2 molecules which act as electron acceptors (5, 14, 15) with the following reactions:

$$\begin{aligned}(O_2)_{gas} &\rightarrow (O_2)_{ads}\\ (O_2)_{ads} + e^- &\rightarrow (O_2^-)_{ads}\\ (O_2^-)_{ads} + e^- &\rightarrow 2(O^-)_{ads}.\end{aligned} \qquad [4]$$

The presence of charged species at the grain surface creates a depletion layer of length equal to the Debye length inside the grain. This model was successful in explaining the increase in resistance when the grain size approached the Debye length (about 3 nm), i.e., when the whole grain became depleted.

A more sophisticated model (4, 9, 16), in which two kinds of grain boundaries were introduced ("necks" without contact with the atmosphere and "grain boundaries" in contact with the atmosphere), was then proposed to explain the changes in conductivity observed in various nanocrystalline samples.

For the two samples studied here (SK and SX), we obtained markedly different conductivities. Sample SK can be considered as insulating, with a conductivity of less than $10^{-8}\,\Omega^{-1}\,cm^{-1}$, while sample SX conductivity was about $0.02\,\Omega^{-1}\,cm^{-1}$ at 100°C after correction for porosity, i.e.,

$$\sigma = \frac{1}{R}\frac{l_c}{A_c}, \qquad [5]$$

where l_c and A_c are the corrected length and area of the cylindrical sample, calculated from the geometric length l and area A by

$$\begin{aligned}l_c &= l(1-p)^{1/3}\\ A_c &= A(1-p)^{2/3}\end{aligned} \qquad [6]$$

where p is the sample porosity expressed in volume fraction.

The average grain size of sample SX is 20 nm, while that of sample SK is 4 nm (12). The microstructure of both

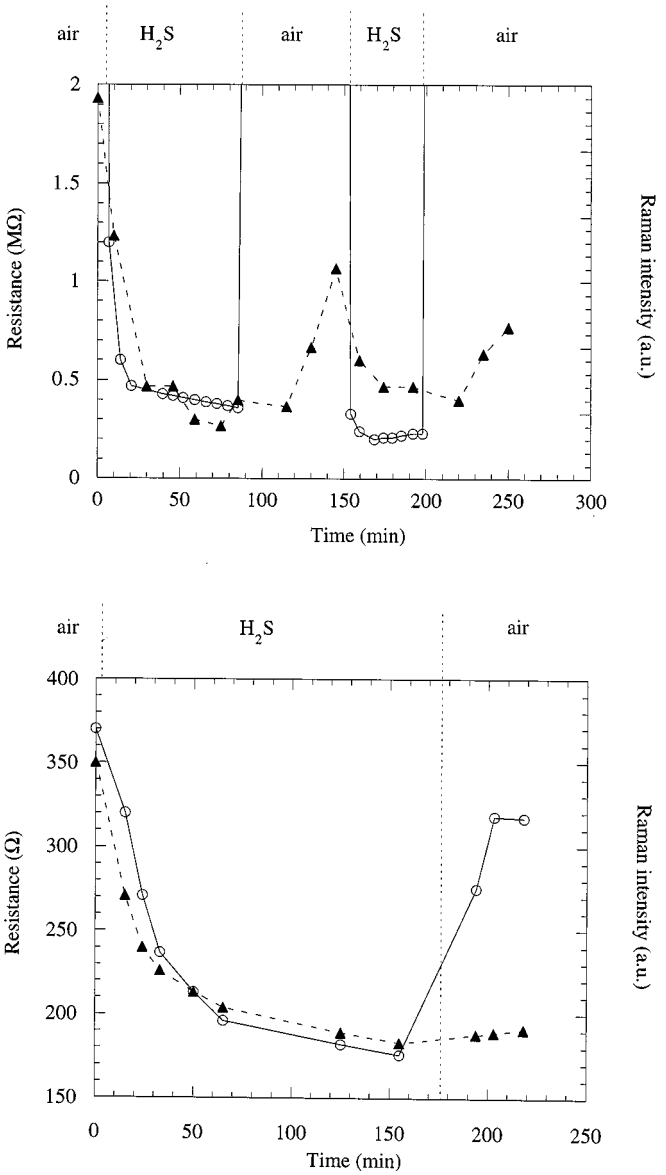

FIG. 8. Changes in the resistance (circles and full line) and in the Raman intensity taken as the absolute intensity of the A_{1g} band (triangles and dotted line) for pellet SK (top) and SX (bottom) as a function of time.

samples is also different. Sample SX shows well-developed three-dimensional aggregates, while sample SK aggregates were two-dimensional plates.

From the above-mentioned experimental work, three nonexclusive explanations can be proposed for the very different conductivities of the two samples.

(i) For any reason, oxygen does not adsorb on sample SX.

(ii) The aggregates density is much higher in the case of sample SX. In this case, interactions with the atmosphere would take place in this sample only at the surface of the aggregates, and not at the crystallite surface. The blocking effect of the depletion layer would therefore be reduced.

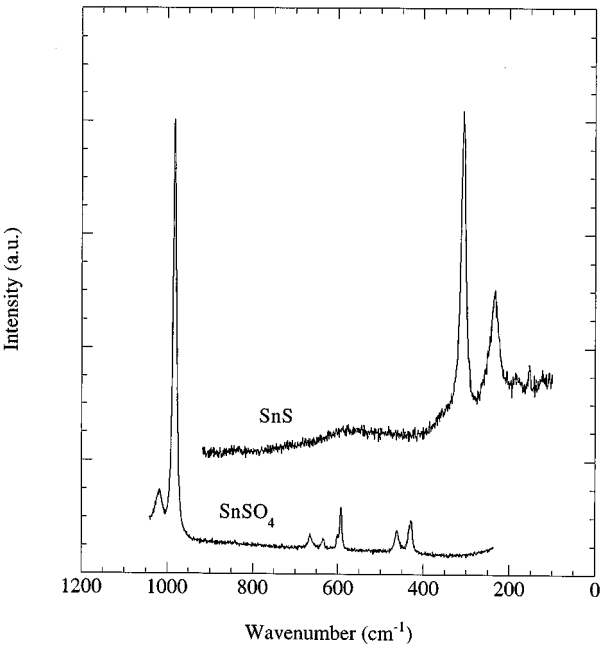

FIG. 9. Raman spectra of pure SnS and $SnSO_4$ at room temperature.

(iii) The number of charge carriers is higher in sample SX, due to a higher amount of oxygen vacancies.

3.4. *Atmospheric Effects on Raman Intensity*

As we stated under Results, the intensity of the A_{1g} band decreases strongly when air is replaced by H_2S. An

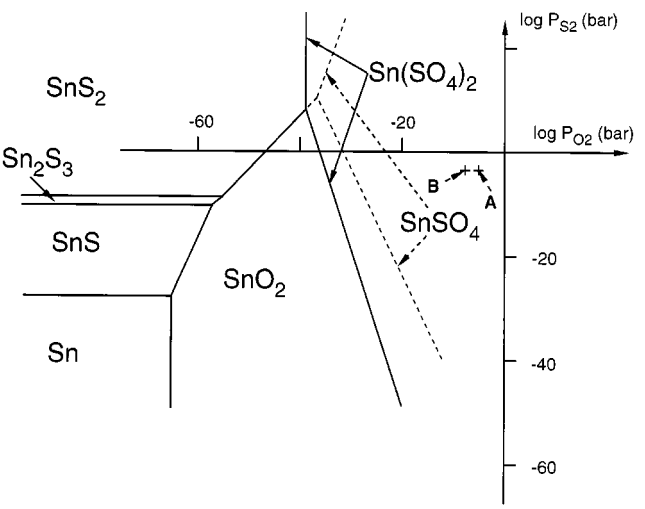

FIG. 10. Stability diagram of tin compounds as a function of S_2 and O_2 partial pressure. The diagram is limited by S_2 condensation for sulfur partial pressures higher than 10^{-8} bar. The $SnSO_4$ metastable phase diagram is also shown in dotted lines. Points A and B are the working points in our experiments, depending on whether we take into account a reaction between H_2S and O_2 (see text for more explanations).

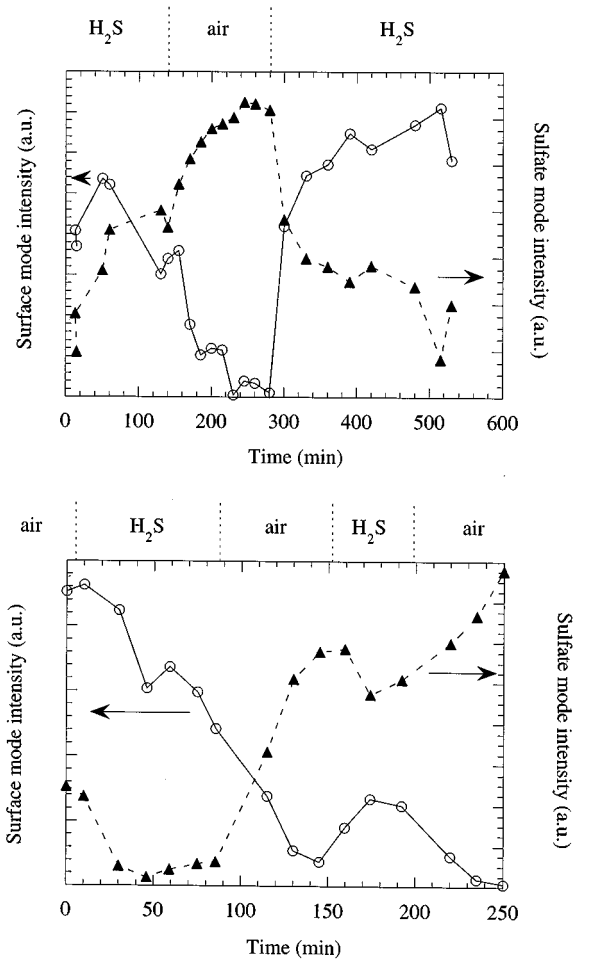

FIG. 11. Changes in the intensities of surface modes (open circles and full lines) and sulfate mode (triangles and dotted lines) for sample SV6 (top) and SK (bottom).

examination of Figs. 3, 4, and 6 shows that this decrease affects most of the Raman features observed on the spectra. If a result of the reaction of SnO_2 with H_2S is the creation of "free" electrons which can absorb the laser light, we may expect a decrease of the whole spectrum intensity.

In addition to this general behavior, there seems to be a strong correlation between the amplitude of the surface mode bands and the amplitude of the sulfate band. Figure 11 shows these amplitudes for samples SV6 and SK, for which a sulfate band is visible. The minima in the surface mode amplitude correspond to maxima of that of the sulfate mode. It is well known (19) that sulfate ions adsorb at the surface of SnO_2 when sulfur containing gases (H_2S, SO_2) are in contact with it. These sulfate ions are linked to the SnO_2 matrix by two quasi-chemical bonds between a superficial oxygen of SnO_2 and an SO_2 entity. We therefore propose that adsorbed sulfate ions freeze partially the surface vibrational modes of sulfur-free SnO_2.

3.5. Origin of the Electrical Resistance Changes

As we mentioned in the Introduction and in Section 3.3, changes in the electrical resistance of SnO_2 are often connected to surface reaction where adsorbed oxygen is replaced by other molecules which do not act as electron acceptors. In our case, the replacement of adsorbed oxygen by adsorbed SO_4 could play this role. However, there seems to be no connection between the presence of adsorbed SO_4 and resistance changes. Sample SX shows resistance changes and no adsorbed SO_4, and sample SK shows adsorbed SO_4 even when the sample is highly resistive. This is particularly clear during the second air–H_2S cycle when the overall Raman spectrum attenuation has been taken into account (Fig. 5). The intensity of the sulfate band remains roughly constant, while changes in the electrical resistance are very important (Fig. 8). On the contrary, the presence of sulfurous (or sulfuric) species is strongly connected to the electrical resistance changes. We already mentioned in Section 2.3 that when switching back to air the resistance change was much quicker than the Raman intensity change. This can be understood if the surface of the grains becomes highly resistive while free electrons still exist in the inner part of the grains. We therefore propose that, when put in contact with H_2S, SnO_2 transforms into SnS_x. This reaction is not solely superficial, but progressively affects the grain in volume. When the sample is put again in contact with air, SnS_x at the surface transforms rapidly into insulating SnO_2, while the SnS_x inside the grain transforms slowly by diffusion of oxygen and sulfur through the surface SnO_2 layer. Such a chemical reaction has also been proposed by Capehart and Chang (20), who found that exposure to H_2S lead to reduced SnO_2.

It is interesting to re-examine the reasons that sample SX was conductive given in Section 3.3 in the light of the proposed model. As SnS_x can be observed in this sample, we must admit that most of the grains can be in contact with the atmosphere and explanation (ii) in Section 3.3 cannot be valid. Although we cannot rule it completely out, explanation (i) is difficult to understand. We have found no reason that oxygen would not absorb on sample SX. The presence of a large amount of oxygen vacancies seems to be a better candidate. In fact, a large amount of oxygen vacancies can be connected to an oxygen ion activity which corresponds to a very reducing atmosphere. It is therefore possible that the formation of sulfate is discouraged by the presence of oxygen vacancies in SnO_2 (see Fig. 10). Another way to figure this is to say that the transformation of H_2S into adsorbed SO_4 implies the oxidation of sulfur and therefore the reduction of SnO_2 following, for example,

$$H_2S + 5O_O^x \rightarrow H_2O + (SO_4)_{ad} + 3V_O^{\bullet\bullet} + 6e', \qquad [7]$$

where $(SO_4)_{ad}$ means adsorbed SO_4, which is composed of SO_2 attached to two oxygens in their normal position. The presence of a large amount of oxygen vacancies would considerably reduce the driving force for this reaction.

Taking into account reaction [7], sulfate formation may play a role in the change in the sample SK resistance during the first air–H_2S cycle, but certainly neither in the other cycles nor in the changes observed with sample SX.

4. CONCLUSION

Four SnO_2 samples were submitted to air–H_2S (300 ppm in Ar) cycles at 100°C and reactions were studied by Raman spectroscopy and resistivity measurements. We observed no change in microcrystalline powder. Three compounds made with nanocrystalline SnO_2 showed changes when exposed to H_2S, as we now summarize. The presence of adsorbed sulfate groups was detected on a powder sample and on an initially highly resistive pellet, but not on an initally conductive sample. We propose that the origin of this effect has to be found in the nonstoichiometry of SnO_2, a high amount of oxygen vacancies being detrimental to the formation of adsorbed SO_4. In all cases, Raman spectra indicate the reversible formation of SnS_x in H_2S atmosphere and this is the origin of the resistiviy change in SnO_2 when in contact with H_2S. Finally, we emphasize that the combination of electrical resistance measurements and of Raman spectroscopy on nanocrystalline materials is very helpful in understanding the chemical processes involved in such reactions.

ACKNOWLEDGMENTS

S. Kondryavtseva and A. Vertegel are kindly acknowledged for the preparation of nanocrystalline materials.

REFERENCES

1. C. G. Fonstad and R. H. Rediker, *J. Appl. Phys.* **42,** 2911 (1971).
2. N. Yamazoe, J. Fuchigami, M. Kishikawa, and T. Seiyama, *Surf. Sci.* **86,** 335 (1979).
3. D. Kohl, *Sensors and Actuators* **18,** 71 (1989).
4. L. Bruno, C. Pijolat, and R. Lalauze, *Sensors and Actuators B* **18–19,** 195 (1994).
5. S. Lenaerts, M. Honoré, G. Huyberechts, J. Roggen, and G. Maes, *Sensors and Actuators B* **18–19,** 478 (1994).
6. V. Lantto, P. Romppainen, T.S. Rantala, and S. Leppävuori, *Sensors and Actuators B* **4,** 451 (1991).
7. G. Martinelli and M.C. Carotta, *Sensors and Actuators B* **18–19,** 720 (1994).
8. H. Ogawa, M. Nishikawa, and A. Abe, *J. Appl. Phys* **53,** 4448 (1982).
9. C. Xu, J. Tamaki, N. Miura, and N. Yamazoe, *Sensors and Actuators B* **3,** 147 (1991).
10. N. Bârsan, *Sensors and Actuators B* **17,** 241 (1994).
11. X. Wang, S.S. Yee, and W.P. Carey, *Sensors and Actuators B* **24–25,** 454 (1995).
12. L. Abello, B. Bochu, A. Gaskov, S. Koudryavtseva, G. Lucazeau, and M. Roumyantseva, *J. Solid State Chem.* **135,** 78 (1998).
13. Z.M. Jarzebski and J.P. Marton, *J. Electrochem.* Soc. **123,** 299C (1976).
14. L. Nanis and G. Advani, *Int. J. Electron.* **52,** 345 (1982).
15. J.N. Zemel, *Thin Solid Films* **163,** 189 (1988).
16. N. Yamazoe and N. Miura, *Chem. Sensors Technol.* **4,** 19 (1992).
17. S.D. Ross, *in* "The Infrared Spectra of Minerals" (V.C. Farmer, Ed.), p. 423. Mineralogical Society Monograph 4. The Mineralogical Society, London, 1974.
18. I. Barin, "Thermochemical Data of Pure Substances." VCH, Weinheim, Germany, 1989.
19. B. Gergely, A. Auroux, B. Bonnetot, and C. Guimon, *in* "Congrès de la Société Française de Chimie, SFC 97" (E.J. Dufourc and C. Sourisseau, Eds.), p. 163. Société Française de Chimie, Paris, France, 1997.
20. T.W. Capehart and S.C. Chang, *J. Vac. Sci. Technol.* **18,** 393 (1981).